Article

Cancer Cell

c-RAF Ablation Induces Regression of Advanced *Kras/Trp53* Mutant Lung Adenocarcinomas by a Mechanism Independent of MAPK Signaling

Graphical Abstract

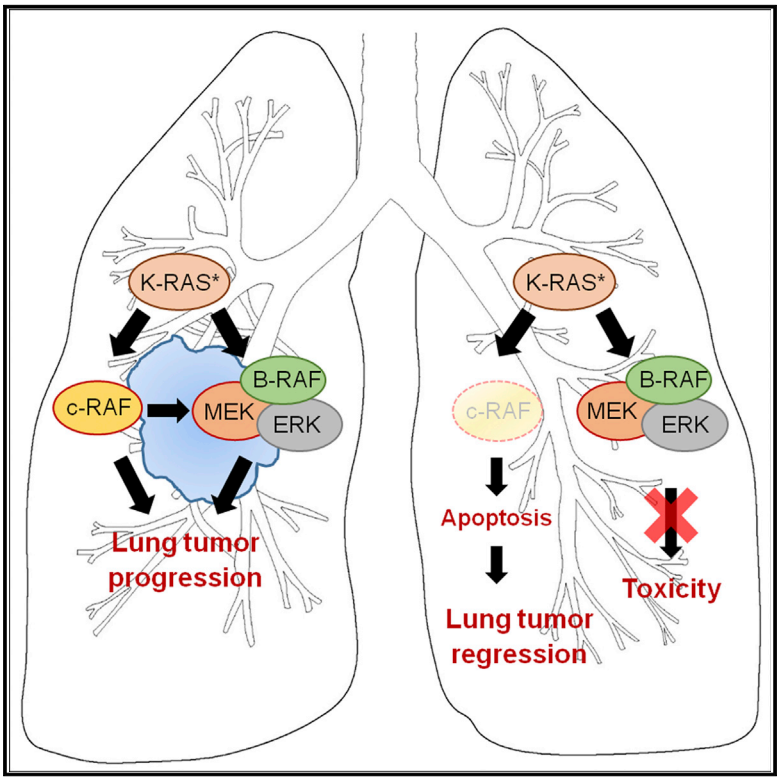

Authors

Manuel Sanclemente, Sarah Francoz, Laura Esteban-Burgos, ..., Matthias Drosten, Monica Musteanu, Mariano Barbacid

Correspondence

mmusteanu@cnio.es (M.M.), mbarbacid@cnio.es (M.B.)

In Brief

Sanclemente et al. generate oncogenic *Kras* mice that allow inducible deletion of *Raf1*, encoding c-RAF, and/or *Braf* in established $Kras^{G12V}$ or $Kras^{G12V}$; $Trp53^{-/-}$ lung tumors. They show that systemic c-RAF ablation has limited toxicity and leads to significant tumor regression without having an impact on MAPK activity.

Highlights

- Ablation of c-RAF expression induces regression of *Kras/Trp53* mutant lung tumors
- Loss of c-RAF expression does not affect MAPK signaling
- Systemic ablation of c-RAF expression in adult mice has limited toxic effects

Sanclemente et al., 2018, Cancer Cell *33*, 217–228
February 12, 2018
https://doi.org/10.1016/j.ccell.2017.12.014

CellPress

Cancer Cell
Article

c-RAF Ablation Induces Regression of Advanced *Kras/Trp53* Mutant Lung Adenocarcinomas by a Mechanism Independent of MAPK Signaling

Manuel Sanclemente,[1,3] Sarah Francoz,[1,3,5] Laura Esteban-Burgos,[1] Emilie Bousquet-Mur,[1,6] Magdolna Djurec,[1] Pedro P. Lopez-Casas,[2] Manuel Hidalgo,[2,7] Carmen Guerra,[1] Matthias Drosten,[1] Monica Musteanu,[1,4,8,*] and Mariano Barbacid[1,4,*]

[1]Molecular Oncology Program
[2]Clinical Research Program
Centro Nacional de Investigaciones Oncológicas (CNIO), Madrid 28029, Spain
[3]These authors contributed equally
[4]Senior author
[5]Present address: Cell and Developmental Biology Area, Centro National de Investigaciones Cardiovasculares (CNIC), Madrid 28029, Spain
[6]Present address: Oncogenic Pathways in Lung Cancer, Institut de Recherche en Cancérologie de Montpellier (IRCM), Montpellier 34298, France
[7]Present address: Division of Hematology-Oncology, Beth Israel Deaconess Medical Center (BIDMC), Boston, MA 02215, USA
[8]Lead Contact
*Correspondence: mmusteanu@cnio.es (M.M.), mbarbacid@cnio.es (M.B.)
https://doi.org/10.1016/j.ccell.2017.12.014

SUMMARY

A quarter of all solid tumors harbor *KRAS* oncogenes. Yet, no selective drugs have been approved to treat these malignancies. Genetic interrogation of the MAPK pathway revealed that systemic ablation of MEK or ERK kinases in adult mice prevent tumor development but are unacceptably toxic. Here, we demonstrate that ablation of c-RAF expression in advanced tumors driven by $Kras^{G12V}$/*Trp53* mutations leads to significant tumor regression with no detectable appearance of resistance mechanisms. Tumor regression results from massive apoptosis. Importantly, systemic abrogation of c-RAF expression does not inhibit canonical MAPK signaling, hence, resulting in limited toxicities. These results are of significant relevance for the design of therapeutic strategies to treat K-RAS mutant cancers.

INTRODUCTION

KRAS mutations have been identified in a quarter of all human cancers, including those with worse prognosis, such as pancreatic ductal adenocarcinoma, colorectal adenocarcinoma, and lung adenocarcinoma. In spite of the advances we have witnessed during the last two decades in the development of targeted therapies, there are still no selective drugs against these malignancies (Cox et al., 2014). Although K-RAS is not a trivial druggable target (Ostrem et al., 2013), most of its downstream effectors are druggable kinases. For instance, the MAPK pathway consists of a cascade of protein kinases that amplify and regulate mitogenic signals. These protein kinases come in three flavors, the RAF kinases (A-RAF, B-RAF, and c-RAF), the MEK kinases (MEK1 and MEK2), and the ERK kinases (ERK1 and ERK2). The latter diversify these mitogenic signals by phosphorylating a wide variety of substrates, including transcription factors as well as other kinases that control cellular processes as distinct as protein synthesis and the cell cycle (Sebolt-Leopold and Herrera, 2004). K-RAS also activates a second kinase cascade via its interaction with the catalytic subunits of PI3K, a group of phosphoinositol kinases responsible for the production

Significance

More than 30 years after the identification of *KRAS* oncogenes in human cancer, there are no selective therapies against these tumors. Direct targeting of K-RAS has proven challenging. Hence, most efforts have focused on targeting its downstream kinases. Here, we report that targeting c-RAF in mice induces significant regression of advanced $Kras^{G12V}$/*Trp53* mutant lung tumors by a mechanism that induces massive apoptosis without affecting canonical MAPK signaling. As a consequence, systemic ablation of c-RAF does not induce the unacceptable toxicities observed when tampering with its downstream kinases, MEK or ERK. These results should open avenues to design effective therapeutic strategies against K-RAS mutant cancers.

of the second messenger PIP3. PIP3 binds and activates a wide variety of proteins, including other protein kinases, such as PDK1 and the AKT kinases that have been implicated in a variety of cellular activities including survival (Castellano and Downward, 2011).

One of the biggest challenges of precision medicine is to develop therapeutic strategies that block oncogenic signaling without affecting normal homeostasis. In mice, ablation of the MEK1/2 kinases effectively prevented K-RAS-driven tumor development. Similar results were obtained upon ablation of the ERK1/2 kinases. Unfortunately, systemic ablation of the MEK1/2 or ERK1/2 kinases in adult mice led to extreme toxicities that resulted in the rapid death of the animals (Blasco et al., 2011). MEK inhibitors have proven to be effective against K-RAS-driven mouse tumors; however, their high toxicities have prevented their approval for their use in human patients. Ablation or inactivation of RAS-mediated PI3K activation has also shown to block progression of K-RAS-driven tumors (Castellano et al., 2013). However, these strategies also induce unacceptable toxicities in adult mice (our unpublished data). Indeed, in spite of intense efforts by the pharmaceutical industry, no PI3K inhibitors have been so far approved to treat K-RAS-driven tumors.

Targeting of c-RAF but not the B-RAF kinase revealed equally effective inhibition of tumor development without inducing significant toxicities (Blasco et al., 2011; Karreth et al., 2011), thus suggesting that these kinase isoforms are likely to play different roles in mediating K-RAS oncogenic signals. In these studies, however, target ablation was concomitant with induction of $Kras^{G12V}$ expression. Hence, they only interrogated the role of these RAF kinases in tumor initiation, not tumor progression, a scenario more relevant to the clinical setting. In this study, we aim to determine the role of c-RAF in lung tumor progression of already established lesions and to assess the effect of its ablation in adult tissue homeostasis.

RESULTS

An Flp/frt-Dependent $Kras^{G12V}$ Oncogene-Driven Lung Adenocarcinoma Model

To determine whether RAF kinases play a role in advanced tumor development without affecting normal adult tissue homeostasis, we have developed a genetically engineered mouse (GEM) model to temporally and spatially separate tumor development from target ablation by using two independent recombinase systems. To this end, we first targeted the *Kras* locus by inserting a Neo-resistant STOP cassette flanked by frt (F) sequences within the first intron, along with a mutated first exon encoding a Gly to Val substitution (see STAR Methods). The resulting strain, $Kras^{+/FSFG12V}$, developed lung adenocarcinomas upon intratracheal infection with adenoviral particles expressing the Flp recombinase (Ad-Flp) (Buchholz et al., 1998) with complete penetrance and latencies similar to those observed in previous studies infecting $Kras^{+/LSLG12Vgeo}$ mice with adenoviral particles expressing the Cre-recombinase (data not shown).

c-RAF Ablation Reduces Tumor Burden in $Kras^{G12V}$-Driven Lung Tumors

$Kras^{+/FSFG12V}$ mice were crossed to animals carrying *Raf1* conditional floxed (L) alleles, hereafter referred to as c-Raf^{L} (Jesenberger et al., 2001), and an inducible ubiquitously expressed CreERT2 recombinase knocked in at the *Polr2a* gene locus, hereafter referred to as $RERT^{ert}$ (Guerra et al., 2003). To evaluate potential compensatory effects by the related B-RAF kinase, we also generated an additional strain containing *Braf* floxed alleles ($Braf^{L}$) (Chen et al., 2006). Exposure of tumor-bearing mice to a tamoxifen (TMX)-containing diet for 4 months allowed us to evaluate the effect of eliminating the c-RAF and/or B-RAF kinases in tumor-bearing mice. This strategy also allowed us to identify potential toxic effects that could result from the systemic elimination of these kinases in normal adult tissues, key information to determine the suitability of this therapeutic strategy.

$Kras^{+/FSFG12V}$;$RERT^{ert/ert}$;c-$Raf^{L/L}$, $Kras^{+/FSFG12V}$;$RERT^{ert/ert}$;$Braf^{L/L}$, and $Kras^{+/FSFG12V}$;$RERT^{ert/ert}$;c-$Raf^{L/L}$;$Braf^{L/L}$ mice were infected with low-titer Ad-Flp particles by intratracheal instillation to allow expression of the resident $Kras^{G12V}$ oncogene in lung tissue. The use of low titers of Ad-Flp particles resulted in the induction of one or very few tumors in each animal in order to facilitate their individual analysis by monthly computed tomography (CT) scans. Mice displaying at least one tumor larger than 1 mm in diameter were fed *ad libitum* with a TMX-containing diet to ablate the conditional c-Raf^{L} and/or $Braf^{L}$ alleles. Previous studies have shown that germ line ablation of c-RAF and B-RAF kinase was embryonic lethal (Huser et al., 2001; Mikula et al., 2001; Wojnowski et al., 1997); however, these kinases do not appear to be essential for adult homeostasis, since adult mice survived well with 4 months of TMX exposure, a time in which expression of these kinases was completely eliminated (Figures 1A and S1A).

All tumors present in control $Kras^{+/FSFG12V}$;$RERT^{ert/ert}$ mice grew in size during this period of time leading to a significant increase in tumor burden and had to be sacrificed at humane endpoint within 6 months (Figures 1B and 1C). Similar results were observed in $Kras^{+/FSFG12V}$;$RERT^{ert/ert}$;$Braf^{L/L}$ animals, indicating that B-RAF kinase does not play a relevant role in mediating $K\text{-}RAS^{G12V}$ oncogenic signals. In contrast, the average tumor burden in $Kras^{+/FSFG12V}$;$RERT^{ert/ert}$;c-$Raf^{L/L}$ and $Kras^{+/FSFG12V}$;$RERT^{ert/ert}$;c-$Raf^{L/L}$;$Braf^{L/L}$ animals decreased significantly after 4 months of TMX exposure (Figures 1B and 1C). At this time, analysis of tissues from these mice did not reveal any obvious alterations, indicating that systemic ablation of c-RAF does not induce significant toxicities. Moreover, all lesions present in these mice were hyperplasias or adenomas (Figures S1B and S1C). Concomitant ablation of c-Raf^{L} and $Braf^{L}$ alleles led to a slightly more pronounced reduction in tumor burden (Figures 1B and 1C). Yet, ablation of both kinases was not well tolerated and all $Kras^{+/FSFG12V}$;$RERT^{ert/ert}$;c-$Raf^{L/L}$;$Braf^{L/L}$ had to be sacrificed during the first 4 months of TMX exposure (Figures 1B and 1C). In contrast, $Kras^{+/FSFG12V}$;$RERT^{ert/ert}$;c-$Raf^{L/L}$ survived for up to 9 months, indicating that systemic loss of c-RAF expression is well tolerated by adult mice. Importantly, loss of c-RAF expression did not result in the development of resistance mechanisms, at least during the length (9 months) of TMX exposure.

Elimination of c-RAF Expression Decreases Glucose Uptake in $Kras^{G12V}$-Driven Lung Tumors

In the clinical setting, tumor progression is often diagnosed by positron emission tomography (PET) scanning, a technique that detects the ability of tumors to metabolize radioactive tracers, most commonly the glucose analogue [^{18}F]-fluoro-2-deoxy-glucose

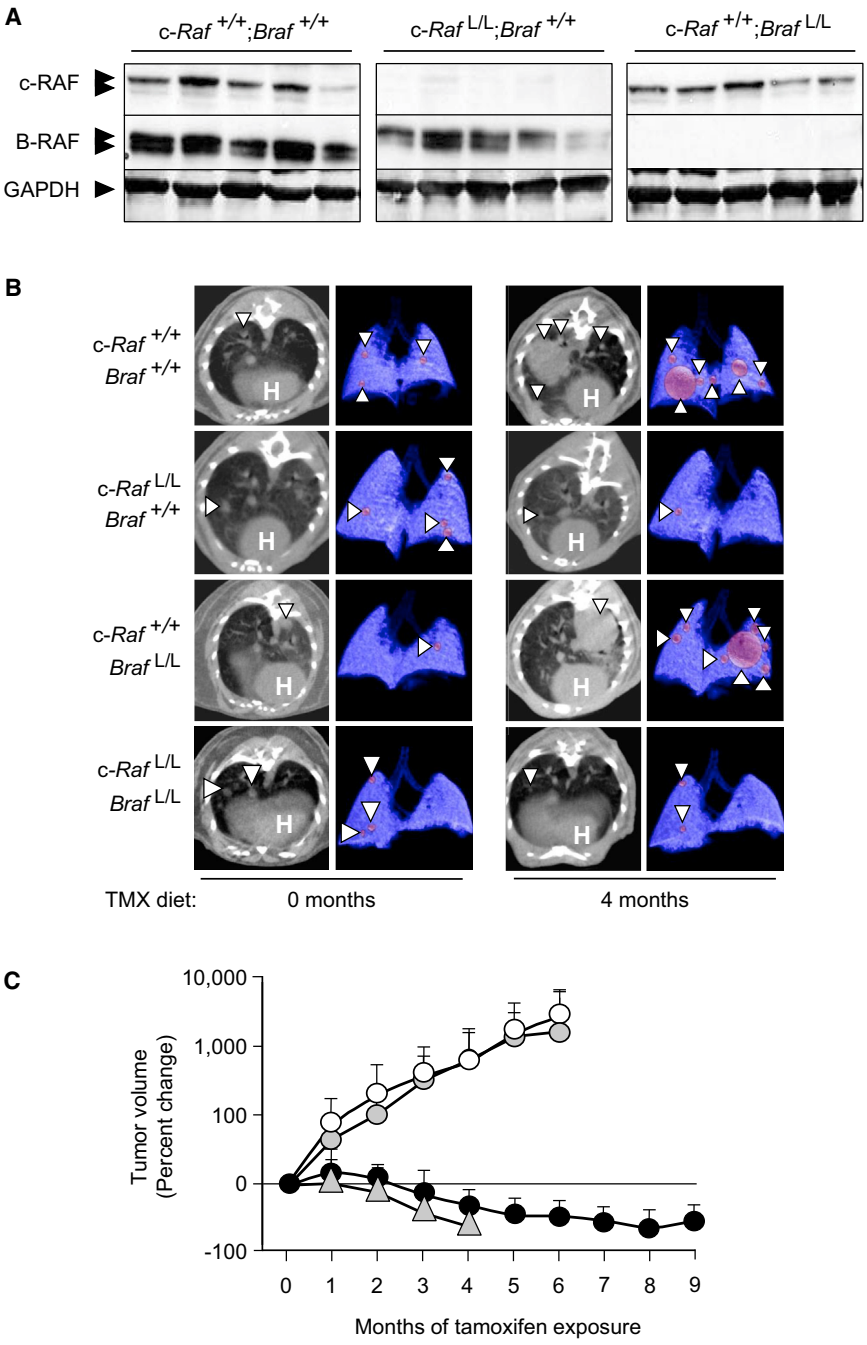

Figure 1. c-RAF Ablation Reduces Tumor Burden in *Kras*^{G12V}-Driven Lung Tumors

(A) Western blot analysis of c-RAF and B-RAF expression in lysates derived from five independent tumors obtained from *Kras*$^{+/FSFG12V}$;*RERT*$^{ert/ert}$, *Kras*$^{+/FSFG12V}$;*RERT*$^{ert/ert}$;c-*Raf*$^{L/L}$ and *Kras*$^{+/FSFG12V}$;*RERT*$^{ert/ert}$;*Braf*$^{L/L}$ mice exposed for 4 months to a TMX diet. GAPDH was used as the loading control. Migration of the above proteins is indicated by arrowheads.

(B) CT scan axial projection images and 3D reconstructions of lungs of representative *Kras*$^{+/FSFG12V}$;*RERT*$^{ert/ert}$ mice carrying the indicated c-*Raf* and *Braf* alleles before and after 4 months of TMX exposure. Tumors are indicated by arrowheads. H, heart.

(C) Quantification of average tumor volume variation (indicated as percent change) during the TMX exposure for the indicated time. Tumors were measured by CT scans. *Kras*$^{+/FSFG12V}$;*RERT*$^{ert/ert}$ (n = 25) (open circles); *Kras*$^{+/FSFG12V}$;*RERT*$^{ert/ert}$;*Braf*$^{L/L}$ (n = 16) (solid gray circles); *Kras*$^{+/FSFG12V}$;*RERT*$^{ert/ert}$;c-*Raf*$^{L/L}$ (n = 22) (solid black circles) and *Kras*$^{+/FSFG12V}$;*RERT*$^{ert/ert}$;c-*Raf*$^{L/L}$;*Braf*$^{L/L}$ (n = 8) (solid gray triangles) mice. Error bars indicate mean ± SEM.

([^{18}F]-FDG) (Dewan et al., 1993; Scheffler et al., 2013). Comparison of PET/CT scan axial projections and 3D reconstruction images of lungs of representative mice taken before and after 2 months of TMX exposure revealed that ablation of c-RAF expression dramatically reduced [^{18}F]-FDG uptake (Figure 2A). In contrast, tumors present in control animals displayed increased [^{18}F]-FDG uptake. These mice were part of three cohorts of 14 *Kras*$^{+/FSFG12V}$;*RERT*$^{ert/ert}$ mice, 19 *Kras*$^{+/FSFG12V}$;*RERT*$^{ert/ert}$;c-*Raf*$^{L/L}$ mice, and 17 *Kras*$^{+/FSFG12V}$;*RERT*$^{ert/ert}$;c-*Raf*$^{L/L}$;*Braf*$^{L/L}$ mice fed with TMX for 2 months. As summarized in Figure 2B, the overall number of PET^{+} tumors doubled in control mice. In contrast, the number of PET^{+} tumors in those mice that either underwent c-RAF or c-RAF + B-RAF ablation decreased by 45% and 60%, respectively. Similar results were obtained when we analyzed the standardized uptake value (SUV) of individual tumors (Figure 2C). Most tumors expressing c-RAF (26/30, 87%) increased their [^{18}F]-FDG uptake at the end of the 2 months of TMX exposure. In contrast, only 3 of the 46 tumors (6.5%) displayed a slightly higher PET signal after c-RAF ablation (Figure 2C). Finally, none of the tumors that underwent concomitant recombination of c-*Raf*^{L} and *Braf*^{L} alleles increased their PET signal (Figure 2C).

c-RAF Ablation Prevents Tumor-Related Deaths and Increases Survival

Individual analysis of 42 tumors present in 22 *Kras*$^{+/FSFG12V}$;*RERT*$^{ert/ert}$;c-*Raf*$^{L/L}$ mice during a 4-month-long TMX exposure further illustrated the therapeutic benefit that resulted from ablation of c-*Raf*^{L} alleles. As shown in Figure 3A, most tumors present in these mice either partially regressed (12/42, 29%) or completely disappeared (14/42, 33%). Moreover, most of the 16 tumors (11/16, 69%) that progressed during the 4-month long trial did not double in size. In contrast, all tumors that could be analyzed by sequential CT scans (35/46, 76%) in control *Kras*$^{+/FSFG12V}$;*RERT*$^{ert/ert}$;c-*Raf*$^{+/+}$ mice increased in size an average of 9.8-fold, with a significant percentage (9/35, 26%) growing more than 10-fold (Figure 3A). The remaining 11 tumors scored in this trial could not be followed by CT due to the development of pulmonary atelectasis, a

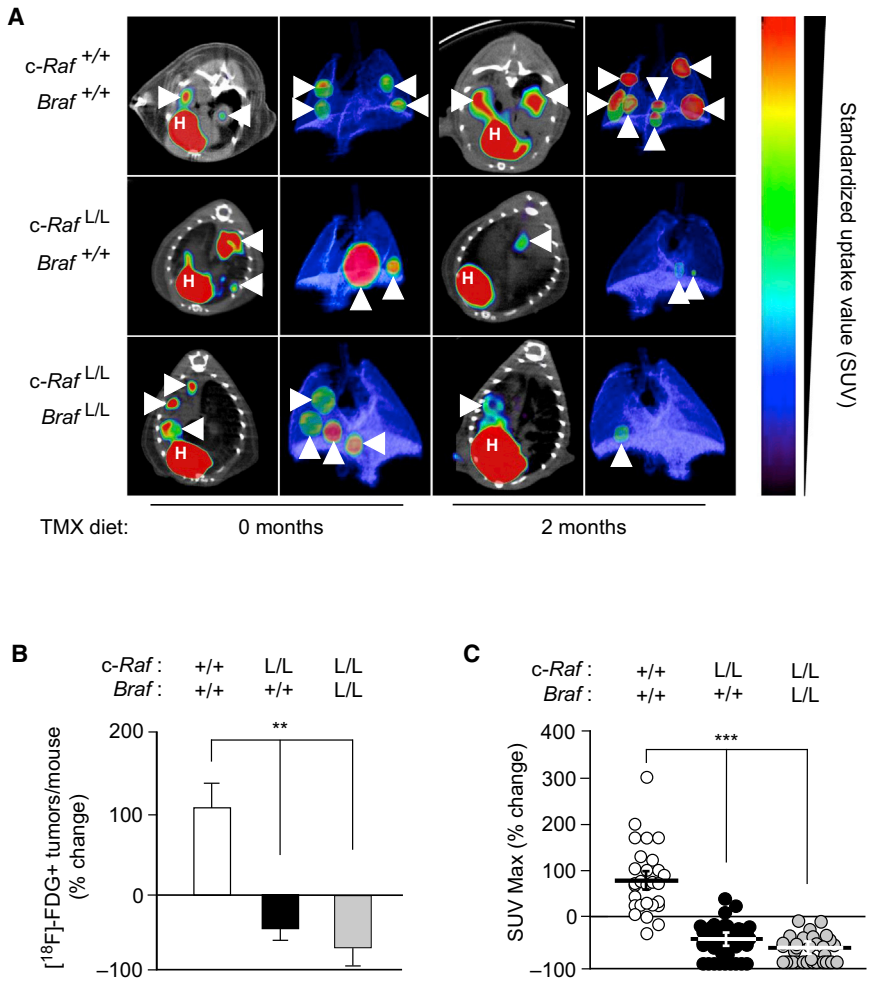

Figure 2. c-RAF Ablation Decreases Glucose Uptake in *Kras*^{G12V}-Driven Lung Tumors

(A) PET/CT scan axial projections images and 3D reconstructions to assess metabolic activity ([^{18}F]-FDG uptake) of representative lungs from *Kras*$^{+/FSFG12V}$;*RERT*$^{ert/ert}$, *Kras*$^{+/FSFG12V}$;*RERT*$^{ert/ert}$;c-*Raf*$^{L/L}$ and *Kras*$^{+/FSFG12V}$;*RERT*$^{ert/ert}$;c-*Raf*$^{L/L}$;*Braf*$^{L/L}$ mice before and after 2 months of TMX exposure. Tumors are indicated by arrowheads. H, heart. Color-scale bar represents SUV of PET.

(B) Quantification, indicated as percent change, of the number of tumors positive for [^{18}F]-FDG uptake per mouse in *Kras*$^{+/FSFG12V}$;*RERT*$^{ert/ert}$ (n = 14) (open bar), *Kras*$^{+/FSFG12V}$;*RERT*$^{ert/ert}$;c-*Raf*$^{L/L}$ (n = 19) (solid black bar), and *Kras*$^{+/FSFG12V}$;*RERT*$^{ert/ert}$;c-*Raf*$^{L/L}$;*Braf*$^{L/L}$ (n = 17) (solid gray bar) mice after 2 months of TMX exposure.

(C) Quantification, indicated as percent change, of the SUV levels of [^{18}F]-FDG uptake per tumor, measured by PET scan, in *Kras*$^{+/FSFG12V}$;*RERT*$^{ert/ert}$ (n = 14 mice/30 tumors) (open circles), *Kras*$^{+/FSFG12V}$;*RERT*$^{ert/ert}$;c-*Raf*$^{L/L}$ (n = 19 mice/46 tumors) (solid black circles), and *Kras*$^{+/FSFG12V}$;*RERT*$^{ert/ert}$;c-*Raf*$^{L/L}$;*Braf*$^{L/L}$ (n = 17 mice/37 tumors) (solid gray circles) animals after 2 months of TMX exposure.

Error bars indicate mean ± SEM. p values were calculated using the unpaired Student's t test. **p < 0.01 or ***p < 0.001. n.s., not significant.

bronchiolar obstruction caused by the expansion of the tumor tissue that ultimately resulted in collapse of the lungs. Finally, whereas 67 tumors appeared during the 4-month-long trial in the control cohort, only 9 *de novo* tumors could be observed in *Kras*$^{+/FSFG12V}$;*RERT*$^{ert/ert}$;c-*Raf*$^{L/L}$ animals. These data are summarized in Figure 3C.

The therapeutic effect of c-RAF ablation resulted in a significant increase in survival. As illustrated in Figure S1A, tumor-bearing *Kras*$^{+/FSFG12V}$;*RERT*$^{ert/ert}$ mice survived an average of 37 weeks after being fed with a TMX-containing diet. Ablation of *Braf*^{L} alleles increased the average survival by 5 weeks in spite of not having a significant effect on tumor progression. Mice in which we eliminated c-*Raf*^{L} alleles increased their survival to 61 weeks, a 65% increase compared with the control cohort (Figure S1A). More importantly, none of the *Kras*$^{+/FSFG12V}$;*RERT*$^{ert/ert}$;c-*Raf*$^{L/L}$ animals analyzed at humane endpoint had advanced adenocarcinomas nor sufficient tumor burden to be cause of death (Figures S1B and S1C). Histopathological analysis of a variety of tissues collected from these mice failed to reveal defined abnormalities. Thus, it is likely that these mice died due to a combination of factors including old age and continuous exposure to TMX for over a year. Yet, we cannot eliminate the possibility that ablation of c-*Raf*^{L} alleles in normal tissues may also contribute to the death of these mice (see below).

c-RAF Is an Effective Therapeutic Target for Advanced *Kras*^{G12V}/*Trp53* Mutant Tumors

Human lung tumors harboring *KRAS* mutations often lack a functional p53 tumor suppressor (Chen et al., 2014). Ablation or inactivation of *Trp53* in *Kras* mutant mice induces more aggressive adenocarcinomas and significantly accelerates tumor development (Jackson et al., 2005). Thus, we interrogated whether ablation of c-RAF expression in *Kras*^{G12V}-driven lung tumors lacking p53 also induced tumor regression. To this end, we added conditional *Trp53* alleles flanked by frt recognition sites (*Trp53*^{F}) to *Kras*$^{+/FSFG12V}$ mice (Lee et al., 2012). Intratracheal infection of *Kras*$^{+/FSFG12V}$;*Trp53*$^{F/F}$ mice with Ad-Flp particles resulted in accelerated tumor development and shortened survival compared with *Kras*$^{+/FSFG12V}$ animals (Figure S2A). As expected, histopathological analysis of their lungs revealed more advanced tumors of higher histological grade (Figure S2B).

Addition of conditional c-*Raf*^{L} alleles to *Kras*$^{+/FSFG12V}$;*Trp53*$^{F/F}$ mice allowed us to interrogate the therapeutic effect of ablating c-RAF expression in a more aggressive tumor environment. Unfortunately, the close proximity of the *Trp53* and the *Polr2a* loci in the mouse genome forced us to replace the *RERT*^{ert} alleles by an h*UBC-CreERT2* transgene in which CreERT2 expression is driven by the human ubiquitin promoter (Ruzankina et al., 2007). To determine the potential toxic consequences of eliminating c-RAF expression under the control

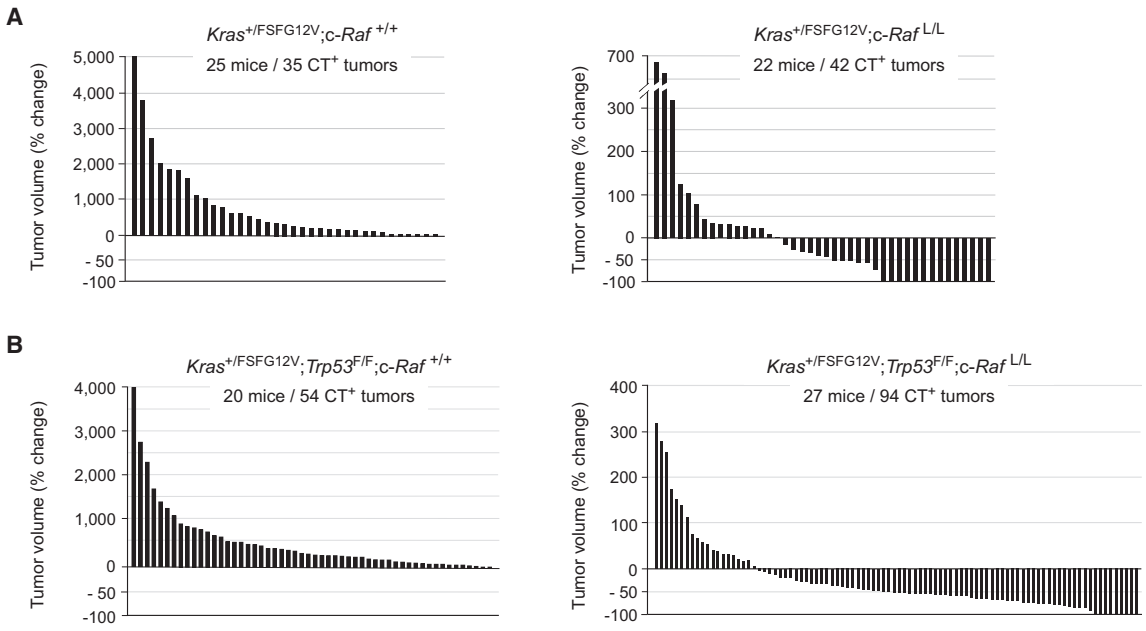

C

	Kras$^{+/FSFG12V}$		*Kras*$^{+/FSFG12V}$;*Trp53*$^{F/F}$	
	c-Raf $^{+/+}$	*c-Raf* $^{L/L}$	*c-Raf* $^{+/+}$	*c-Raf* $^{L/L}$
CT$^+$ Tumors analyzed	35	42	54	94
Partial regression	0	12 (29%)	0	65 (69%)
Complete regression	0	14 (33%)	0	9 (10%)
De novo CT$^+$ tumors	67	9	44	7

Figure 3. c-RAF Is an Effective Therapeutic Target for Advanced *Kras*^{G12V}/*Trp53* Mutant Tumors

(A) (Left) Waterfall plot representing the percent change in tumor volume of individual tumors from *Kras*$^{+/FSFG12V}$;*RERT*$^{ert/ert}$ mice (n = 25 mice/35 tumors) exposed to TMX for 4 months. (Right) Waterfall plot representing the percent change in tumor volume of individual tumors present in *Kras*$^{+/FSFG12V}$;*RERT*$^{ert/ert}$;c-*Raf*$^{L/L}$ mice (n = 22 mice/42 tumors) exposed to TMX for 4 months. The percent change in tumor volume was calculated by CT measurements performed for each individual tumor at the beginning and end of the 4-month-long trial.

(B) Waterfall plot representing the change in tumor volume of individual CT$^+$ tumors present in *Kras*$^{+/FSFG12V}$;*Trp53*$^{F/F}$;h*UBC-CreERT2*$^{+/T}$;c-*Raf*$^{+/+}$ mice (n = 20 mice/54 tumors) exposed to TMX for 2 months. (Right) Waterfall plot representing the change in tumor volume of individual CT$^+$ tumors present in *Kras*$^{+/FSFG12V}$;*Trp53*$^{F/F}$;h*UBC-CreERT2*$^{+/T}$;c-*Raf*$^{L/L}$ mice (n = 27 mice/94 tumors) exposed to TMX for 2 months. The percent change in tumor volumes were calculated for each individual tumor based on CT scans performed at the beginning and at the end of the 2-month-long trial.

(C) Table resuming the numbers of regressing and *de novo* detected tumors in the upper mentioned mice after exposure to TMX.

of the CreERT2-expressing transgene (compared with the *RERT*^{ert} alleles), we exposed 4-month-old, non-tumor-bearing *Kras*$^{+/+}$;*Trp53*$^{F/F}$;h*UBC-CreERT2*$^{+/T}$;c-*Raf*$^{L/L}$ mice to a TMX-containing diet for 2 months. Southern blot analysis of DNA extracted from representative tissues revealed complete c-*Raf* ablation in most organs (Figure S3A). No signs of toxicity were observed in these mice during the 2-month-long exposure, indicating that c-RAF ablation is well tolerated. However, 7-month-old animals died after 18 months of continuous exposure to a TMX diet (Figure S3B). This long-term toxicity was also observed in mice carrying wild-type *c-Raf* alleles, indicating that this toxicity was primarily a consequence of the prolonged exposure to TMX. However, these control mice lived a bit longer (36% longer medium survival), suggesting that c-RAF ablation may also contribute to the premature death of these mice (Figure S3B). Careful postmortem histopathological analysis of both mouse cohorts revealed no significant differences or obvious tissue damage (Figure S3C). Thus, pharmacological inhibition of c-RAF expression is likely to result in acceptable toxicities in a clinical setting.

Next, we designed an experimental trial in which we infected with low titer of Ad-Flp particles two cohorts of *Kras*$^{+/FSFG12V}$;*Trp53*$^{F/F}$;h*UBC-CreERT2*$^{+/T}$ mice carrying either c-*Raf*^{L} or c-*Raf*$^{+}$ alleles. These mice developed a total of 94 and 79 CT-positive, measurable tumors, respectively, between 5 and 6 months post infection (Figure 3B). These mice were then exposed to a TMX diet for 2 months. None of these tumor-bearing mice showed signs of toxicities during this time as determined by the lack of significant body weight loss (Figure S3D). In addition, the overall appearance of the animals was comparable in both cohorts (Figure S3E). Tumor evolution was followed by CT analysis for the duration of the 2-month-long trial. In the case of the control cohort, the appearance of pulmonary atelectasis prevented us from establishing the evolution of 25 lesions, thus limiting our analysis to 54 CT$^+$ c-RAF-expressing control tumors. No such phenomena were

observed in the experimental cohort carrying conditional c-*Raf*^{L} alleles, probably due to the reduced tumor burden. Indeed, the large majority of the 94 CT^{+} tumors present in this experimental cohort either partially regressed (65/94, 69%) or completely disappeared (9/94, 10%) (Figure 3B). Moreover, the 20 tumors (21%) that progressed during the trial grew very slowly and did not even double in size. In contrast, the 54 tumors that could be analyzed in the control mice that carried c-*Raf*$^{+}$ alleles increased in size an average of 6.5-fold (Figure 3B). Moreover, whereas these control mice developed 44 *de novo* tumors during the 2-month-long trial, we only detected seven new tumors in those mice carrying conditional c-*Raf*^{L} alleles (Figure 3C).

These results, taken together, indicate that c-RAF expression is also essential for tumor progression in the absence of the p53 tumor suppressor. Not surprisingly, the number of complete regressions observed in these advanced *Kras*^{G12V}/*Trp53* mutant tumors was lower than in those that retained a functional p53 tumor suppressor (10% versus 33%) (Figure 3C). However, we still observed a significant decrease in the number of adenocarcinomas present in these mice as compared to those scored in the control cohort (Figure S4A). This reduction in aggressive tumors is likely to be due to a significant decrease in the proliferation rate of those tumor cells lacking c-RAF expression, as determined by Ki67 immunohistochemical (IHC) staining (Figure S4B).

In summary, these results predict that inhibition of c-RAF expression/activity should have a significant therapeutic effect in the treatment of patients suffering from K-RAS mutant lung adenocarcinomas.

Pleiotropic Consequences of c-RAF Ablation

Previous studies have shown that recruitment of immune cells plays a role in the regression of lung tumors (DuPage and Jacks, 2013; DuPage et al., 2012). Moreover, a recent study showed that *Kras*^{G12D} expression in resident myeloid cells can lead to mixed lung neoplasms (Kamata et al., 2017). We have not observed these mixed neoplasms possibly due to the fact that the limited levels of adenoviral particles used in our model resulted in the activation of *Kras*^{G12V} expression in a very small number of myeloid cells. On the other hand, tumors of TMX-exposed *Kras*$^{+/FSFG12V}$;*RERT*$^{ert/ert}$;c-*Raf*$^{L/L}$ mice displayed high levels of infiltrating CD3^{+} T lymphocytes, a phenomenon not observed in control tumors that retained c-RAF expression (Figure S4C). In addition, most tumors showed increased levels of CD8^{+} cytotoxic T cells upon c-RAF ablation (Figure S4D). Finally, c-RAF depleted tumors showed a slight decrease in the number of infiltrating macrophages when compared with control tumors (Figure S4E). To what extent these inflammatory responses play a role in tumor regression remains to be determined.

MAPK and PI3K Signaling in *Kras*^{G12V}/*Trp53* Mutant Tumors after Ablation of c-RAF Expression

Next, we interrogated the status of the MAPK and PI3K signaling pathways in *Kras*^{G12V}/*Trp53* mutant lung tumors upon ablation of the c-*Raf*^{L} alleles (Figures 4A–4C). Western blot analysis of tissue extracts obtained from four "Progressor" tumors (P1 to P4) that increased in size during the 2-month-long trial revealed that three of them (P1-P3) retained c-RAF expression levels between 50% and 100% of those tumors that carried wild-type c-*Raf* alleles (C1-C4) (Figure 4A). The increase in size of these P1-P3 "Progressor" tumors is likely to result from c-RAF expression driven by unrecombined c-*Raf*^{L} alleles. As expected, these tumors exhibited normal levels of phospho-MEK, phospho-ERK, and phospho-AKT, indicating the presence of active MAPK and PI3K pathways (Figure 4A). In contrast, most of the cells (>90%) in tumor P4 had lost c-RAF expression. Yet, they retained normal levels of phospho-MEK, phospho-ERK, and phospho-AKT, suggesting that either the other RAF kinase isoforms or possibly other signaling pathways have compensated for the absence of c-RAF expression to sustain MAPK and PI3K activity during tumor progression.

Next, we analyzed eight representative "Regressor" tumors that decreased in size during the trial, including five tumors (R4-R8) that decreased in size more than 50% of their initial volume (Figure 4B). Interestingly, tumors R7 and R8, those tumors displaying the largest regression levels (75%–80% reduction in size, respectively) retained normal levels of c-RAF expression. Likewise, the levels of phospho-MEK, phospho-ERK, and phospho-AKT were mostly comparable to those present in c-RAF-expressing tumors. It is possible that these tumors represent a subpopulation of cells in which c-*Raf* was not efficiently eliminated. If so, we can assume that all tumor cells in which c-RAF was ablated had undergone apoptosis (Figure 4B).

Five of the eight "Regressor" tumors (R2-R6) had minimal levels of c-RAF expression (5%-10% of controls). Yet, four of them (R2, R4-R6) displayed enhanced activation of the MAPK pathway as determined by the increased levels of phospho-MEK and phospho-ERK proteins (Figure 4A). No significant variations were observed in the levels of phospho-AKT. Only one "Regressor" tumor, R3, failed to express detectable levels of phosphorylated MEK and ERK proteins, a result concordant with the established hypothesis that c-RAF mediates MAPK activity. The levels of phospho-AKT expression were similar to those of c-RAF-expressing control tumors, suggesting that the PI3K pathway remained active in the R3 regressing tumor (Figure 4A).

These unexpected observations prompted us to examine phospho-ERK expression by IHC analysis in an additional subset of eight tumors from the same cohort, including one "Progressor" (P5) and seven "Regressor" tumors that underwent regression levels between 40% and 80% (R9-R15) (Figure 4B). As illustrated in Figure 4C, all tumors displayed levels of phospho-ERK positive cells, at least comparable to those observed in control tumors that carried wild-type c-*Raf* alleles (C5-C10) (Figure 4D). In addition, phospho-ERK expression did not correlate with proliferation as determined by KI67 IHC (Figure S5). The lack of c-RAF antibodies suitable for IHC analysis did not allow us to determine whether these phospho-ERK-positive cells retained c-RAF expression. Likewise, the limited amount of tissue prevented us from establishing the levels of c-RAF expression in these tumors by Western blot analysis. Finally, we observed increased expression levels of K-RAS as well as of their other RAS isoforms, H-RAS and/or N-RAS in some tumors (Figure 4A). Yet, these alterations did not correlate with their therapeutic response to c-RAF ablation.

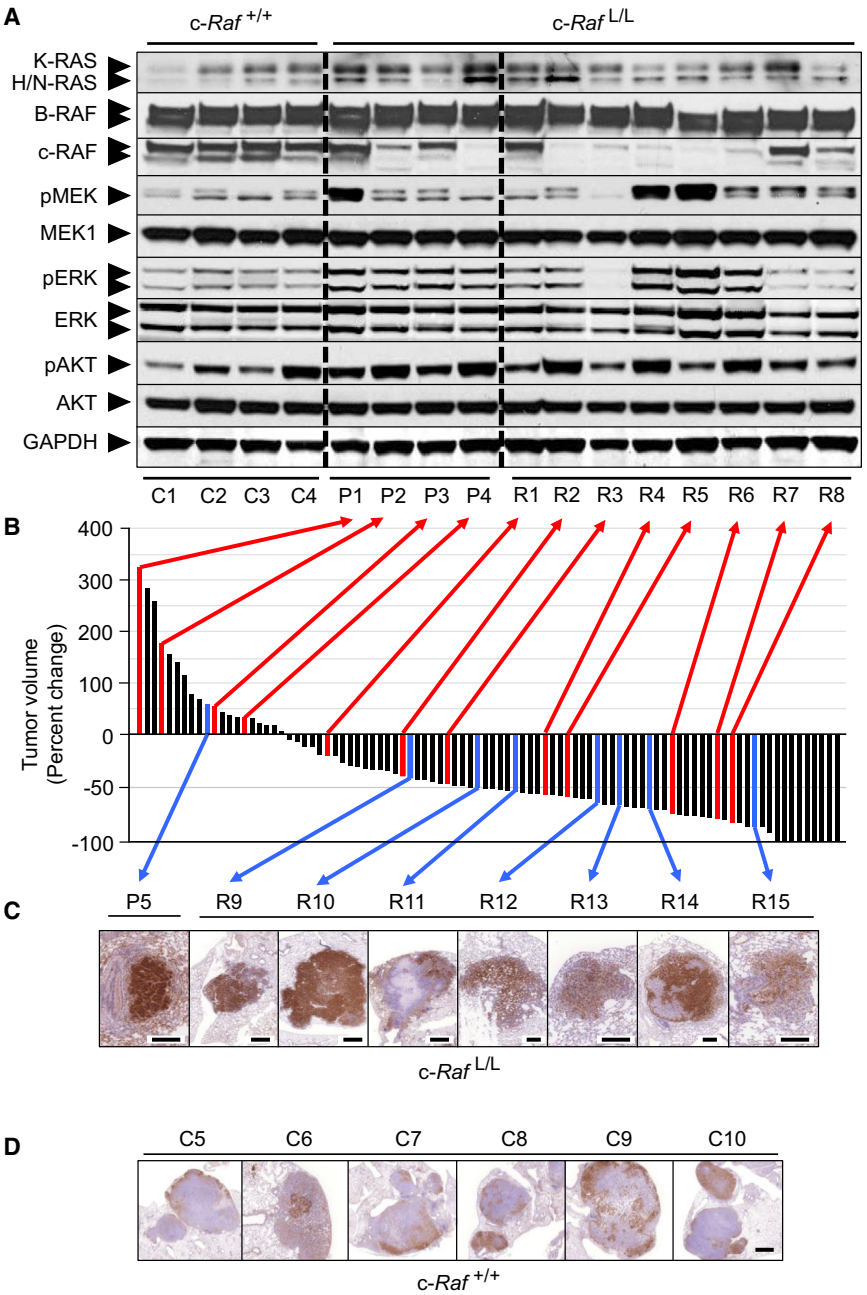

Figure 4. MAPK and PI3K Signaling in *Kras*^{G12V}/*Trp53* Mutant Tumors after c-RAF Ablation

(A) Western blot analysis of K-RAS, H/N-RAS, B-RAF, c-RAF, phospho-MEK (pMEK), MEK1, phospho-ERK (pERK), ERK1/2, phospho-AKT (pAKT), and AKT expression in lysates derived from individual tumors (C1 to C4) of control *Kras*$^{+/FSFG12V}$;*Trp53*$^{F/F}$;h*UBC-CreERT2*$^{+/T}$;c-*Raf*$^{+/+}$ mice and of *Kras*$^{+/FSFG12V}$;*Trp53*$^{F/F}$; h*UBC-CreERT2*$^{+/T}$;c-*Raf*$^{L/L}$ mice exposed to TMX for 2 months. Progressor (P1-P4) and regressor (R1-R8) tumors analyzed are indicated. GAPDH was used as loading control. Migration of the above proteins is indicated by arrowheads.

(B) Waterfall plot representing the change in tumor volume of individual tumors of *Kras*$^{+/FSFG12V}$;*Trp53*$^{F/F}$;h*UBC-CreERT2*$^{+/T}$;c-*Raf*$^{L/L}$ mice previously shown in Figure 3. Tumors used for western blot analysis are indicated in red. Tumors used for phospho-ERK IHC analysis are indicated in blue. The scale used to represent tumor reduction is magnified 2-fold for better visualization.

(C) Phospho-ERK staining of representative sections obtained from the indicated tumors obtained from *Kras*$^{+/FSFG12V}$;*Trp53*$^{F/F}$; h*UBC-CreERT2*$^{+/T}$; c-*Raf*$^{L/L}$ mice treated with TMX for 2 months. Scale bars, 1 mm (R9 to R11 tumors) and 0.2 mm (P5, R12 to R15 tumors).

(D) Phospho-ERK IHC staining of representative tumor sections from tumors (C5 to C10) obtained from *Kras*$^{+/FSFG12V}$;*Trp53*$^{F/F}$;h*UBC-CreERT2*$^{+/T}$; c-*Raf*$^{+/+}$ mice exposed to TMX for 2 months. IHC of the sections depicted in (C) and (D) was carried out in parallel. Scale bar, 2 mm.

c-RAF Ablation Induces Tumor Differentiation and Apoptosis through MAPK Kinase-Independent Mechanisms

Previous studies have indicated that ablation of c-RAF in skin tumors induced by constitutively active SOS, a Ras GDP/GTP exchange factor, provokes tumor regression by a mechanism involving cell differentiation mediated by activation of the ROK-α kinase and subsequent phosphorylation of downstream targets, such as Cofilin (Ehrenreiter et al., 2009; Niault and Baccarini, 2010). In our lung tumor model, c-RAF depleted tumors also exhibited increased numbers of phospho-Cofilin-positive cells compared with control lesions (Figure 5A). Since phosphorylation of Cofilin is associated with cell differentiation, it is likely that ablation of c-RAF expression might contribute to tumor regression and reduction of the number of advanced adenocarcinomas by inducing differentiation of lung tumor cells (Ehrenreiter et al., 2009).

c-RAF had also been shown to promote tumor development by inhibiting apoptosis (Matallanas et al., 2011). IHC analysis of cleaved Caspase 3 expressed in tumors of *Kras*$^{+/FSFG12V}$;*Trp53*$^{F/F}$;h*UBC-CreERT2*$^{+/T}$;c-*Raf*$^{L/L}$ mice displayed a 3-fold increase in the number of apoptotic cells compared with control tumors that expressed c-RAF (Figure 5B). To determine whether these observations were cell autonomous, we established cell lines from tumors of *Kras*$^{+/FSFG12V}$;*Trp53*$^{F/F}$;h*UBC-CreERT2*$^{+/T}$;c-*Raf*$^{L/L}$ mice not exposed to TMX, so we could eliminate c-RAF expression *in vitro* by adding 4-hydroxy-tamoxifen (4OHT) to the media. Indeed, Cre-mediated recombination of the floxed c-*Raf*^{L} alleles *in vitro* proceeded much more efficiently than *in vivo*, leading to complete absence of c-RAF expression within 48 hr in three independent cell lines. As illustrated in Figure 5C, ablation of c-RAF expression triggered the rapid induction of apoptosis in a dose-dependent manner. Concomitantly with loss of c-RAF expression, we observed a decrease in Caspase 3 levels along with the appearance of robust levels of cleaved Caspase 3 (Figure 5C).

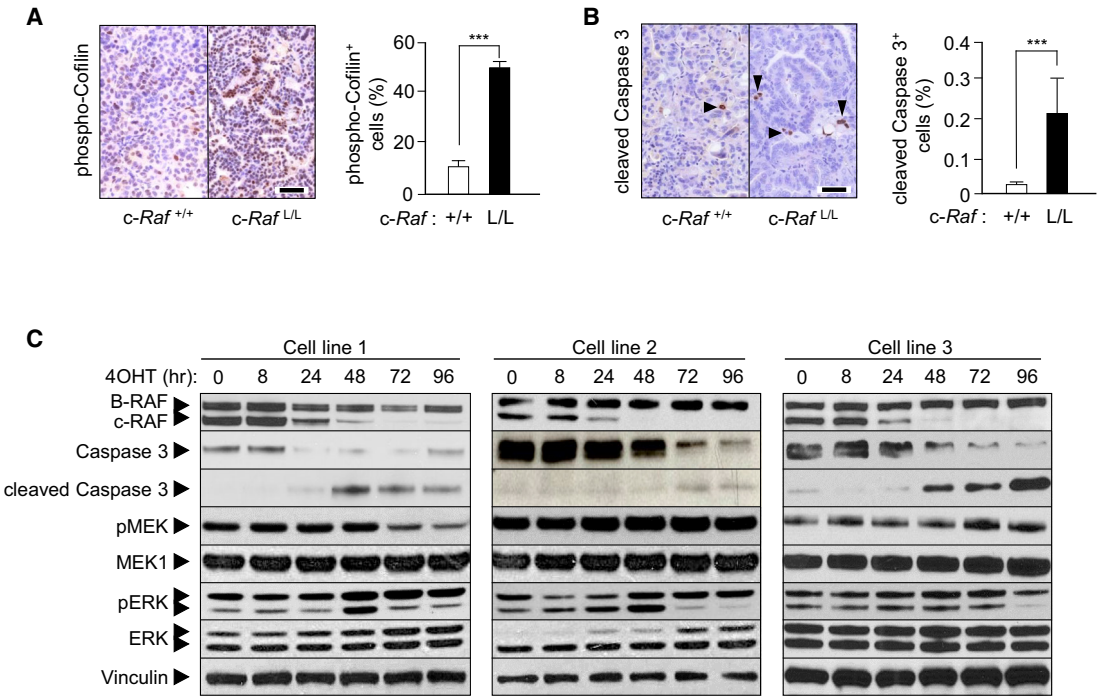

Figure 5. c-RAF Ablation Induces Tumor Differentiation and Apoptosis through MAPK Independent Mechanisms

(A) (Left) Phospho-Cofilin staining and (right) quantification of phospho-Cofilin^{+} cells in representative sections of paraffin-embedded tumors of *Kras*$^{+/FSFG12V}$;*Trp53*$^{F/F}$;h*UBC-CreERT2*$^{+/T}$;c-*Raf*$^{+/+}$ (+/+, open bar) and *Kras*$^{+/FSFG12V}$;*Trp53*$^{F/F}$;h*UBC-CreERT2*$^{+/T}$;c-*Raf*$^{L/L}$ (L/L, solid bar) mice (n = 6 per genotype) exposed to TMX for 2 months. Scale bar, 0.05 mm.

(B) (Left) Cleaved Caspase 3 staining and (right) quantification of cleaved Caspase 3^{+} cells in representative sections of paraffin-embedded tumors of *Kras*$^{+/FSFG12V}$;*Trp53*$^{F/F}$;h*UBC-CreERT2*$^{+/T}$;c-*Raf*$^{+/+}$ (+/+, open bar) and *Kras*$^{+/FSFG12V}$;*Trp53*$^{F/F}$;h*UBC-CreERT2*$^{+/T}$;c-*Raf*$^{L/L}$ (L/L, solid bar) mice (n = 6 per genotype) exposed to TMX for 2 months. Cleaved Caspase 3^{+} cells are indicated by arrowheads. Scale bar, 0.05 mm.

(C) Western blot analysis of B-RAF, c-RAF, Caspase 3, cleaved Caspase 3, phospho-MEK, MEK1, phospho-ERK and ERK expression in lysates from *Kras*^{G12V};*Trp53*$^{-/-}$;h*UBC-CreERT2*$^{+/T}$;c-*Raf*$^{L/L}$ cells maintained in 4OHT-containing media. Samples were harvested at the indicated times in hr. Vinculin was used as loading control. Migration of the above proteins is indicated by arrowheads. Three independent tumor cell lines from three different animals were evaluated.

Error bars indicate mean ± SEM. p values were calculated using the unpaired Student's t test. ***p < 0.001.

In contrast, loss of c-RAF expression had no effect on the levels of phospho-MEK and phospho-ERK expression, thus confirming our *in vivo* observations that loss of c-RAF expression had no effect on the activation of the MAPK pathway (Figure 5C). These results, taken together, illustrate that c-RAF promotes tumor progression by mechanisms that do not involve the MAPK pathway.

c-RAF Expression Is Essential for Proliferation of Patient-Derived Xenograft Tumors

To determine whether our results could be translated to a human scenario, we established primary lung tumor cell lines from two patient-derived xenograft (PDX) tumor models. Both PDX-derived cell lines (PDX-dc) express the oncogenic *KRAS*^{G12C} mutation. In order to evaluate the role of c-RAF expression in proliferation, cells were infected with lentiviruses expressing either a short hairpin RNA (shRNA) against c-RAF or a scrambled shRNA as control. Endogenous c-RAF expression was significantly downregulated 2 weeks after the infection with the shRNA against c-RAF but not affected by the control shRNA (Figure S6). Infection of both PDX-dc with lentiviral particles expressing the shRNA against c-RAF resulted in complete (PDX-dc1) and partial (PDX-dc2) inhibition of cell growth, respectively (Figures 6A and 6D). Next, we injected infected PDX-dc1and PDX-dc2 cells into the lung parenchyma of immune-compromised mice. As illustrated in Figure 6B, PDX-dc1 cells expressing the c-RAF shRNA formed significantly fewer tumors than those elicited by cells containing the scrambled shRNA. Moreover, these tumors were of significantly smaller size (Figure 6C). PDX-dc2 cells expressing the c-RAF shRNA also displayed growth inhibition, albeit not as dramatic as that observed with PDX-dc1 cells (Figure 6D). These cells induced a slight decrease in tumor number and volume than control cells expressing the scrambled shRNA (Figures 6E and 6F).

To evaluate if the dramatic effect on growth inhibition observed in PDX-dc1 cells was specifically due to c-RAF downregulation, we infected these cells with lentiviruses expressing either a murine c-*Raf* cDNA or an empty vector. Once cells resumed proliferation, they were infected with lentiviruses expressing either an shRNA against human c-RAF sequences to deplete endogenous c-RAF expression or with a scrambled shRNA as a negative control. All cells infected with the scrambled shRNA formed similar numbers of colonies regardless of the presence of the murine c-*Raf* sequences since they retained endogenous c-RAF expression

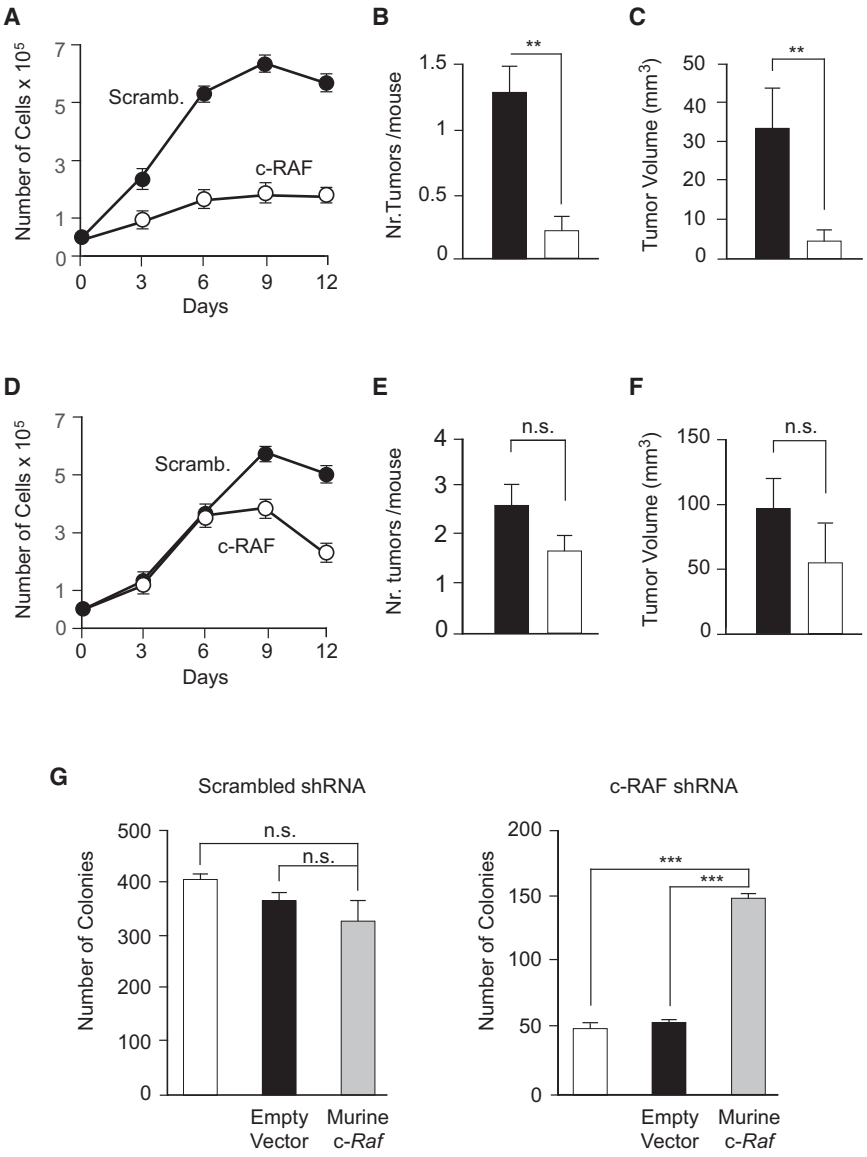

Figure 6. c-RAF Expression Is Essential for Proliferation of Patient-Derived Xenograft Tumors

(A) Cell proliferation assay of a PDX-derived cell line (PDX-dc1 harboring K-RAS^{G12C} mutation) expressing scrambled shRNA (Scramb.) (solid circles) and shRNA against c-RAF (c-RAF) (open circles).

(B) Quantification of tumor number per mouse after orthotopic implantation of PDX-dc1 expressing scrambled shRNA (solid bar) and shRNA against c-RAF (open bar) in nude mice. Animals were analyzed at 5 weeks after the implantation. n = 10 mice/condition.

(C) Quantification of tumor volume after orthotopic implantation of PDX-dc1 expressing scrambled shRNA (solid bar) and shRNA against c-RAF (open bar) in nude mice. Animals were analyzed at 5 weeks after the implantation. n = 10 mice/condition.

(D) Cell proliferation assay of a PDX-derived cell line (PDX-dc2 harboring K-RAS^{G12C} mutation) expressing scrambled shRNA (Scramb.) (solid circles) and shRNA against c-RAF (c-RAF) (open circles).

(E) Quantification of tumor number per mouse after orthotopic implantation of PDX-dc2 expressing scrambled shRNA (solid bar) and shRNA against c-RAF (open bar) in nude mice. Animals were analyzed at 3 weeks after the implantation. n = 7 mice/condition.

(F) Quantification of tumor volume after orthotopic implantation of PDX-dc1 expressing scrambled shRNA (solid bar) and shRNA against c-RAF (open bar) in nude mice. Animals were analyzed at 3 weeks after the implantation. n = 7 mice/condition.

(G) (Left) Quantification of colonies forming in PDX-dc1 cells, PDX-dc1 cells expressing lentiviral pLVX control particles (empty vector) or expressing the wild-type murine c-*Raf* (Murine c-*Raf*) (as indicated). All cells indicated are expressing a scrambled shRNA. (Right) Quantification of colonies forming in PDX-dc1 cells, PDX-dc1 cells expressing lentiviral pLVX control particles (empty vector) or expressing the wild-type murine c-*Raf* (Murine c-*Raf*) (as indicated). All cells indicated are expressing a shRNA against human c-RAF.

Error bars indicate mean ± SEM. p values were calculated using the unpaired Student's t test. **p < 0.01 or ***p < 0.001. n.s., not significant.

(Figure 6G). In contrast, those PDX-dc1 cells devoid of endogenous c-RAF only formed a significant number of colonies in the presence of the murine c-*Raf* sequences (Figure 6G). Taken together, these results indicate that c-RAF expression is also essential for growth of at least some human lung adenocarcinomas.

DISCUSSION

In spite of intense research efforts, K-RAS mutant tumors remain intractable for targeted therapies. Pharmaceutical companies have developed selective inhibitors against most, if not all, druggable K-RAS effectors. Yet, none of them have been approved by the US Food and Drug Administration. Genetic interrogation of the potential therapeutic value of K-RAS effectors within the MAPK signaling pathway has revealed three classes of targets: those that have no effect in preventing the development of K-RAS-driven lung adenocarcinoma (A-RAF, B-RAF, CDK2, and CDK6), those that prevent tumor development but cause unacceptable toxicities if eliminated systemically (MEK1/2, ERK1/2, and CDK1), and those that prevented tumor development (c-RAF and CDK4) when ablated concomitantly with *Kras* oncogene expression and do not induce significant toxicities when targeted systemically (Blasco et al., 2011; Karreth et al., 2011; Puyol et al., 2010). These observations, taken together, suggest that genetic studies may serve to guide more rational approaches to the development of targeted therapies against K-RAS-driven tumors.

To this end, we have now interrogated the therapeutic effect of ablating c-*Raf* expression in pre-existing, advanced lung

adenocarcinomas driven by *Kras*^{G12V}/*Trp53* mutations. As illustrated here, c-RAF ablation provides significant therapeutic benefit, leading to partial regression of most tumors, including some cases in which the tumor completely disappeared. As a consequence, tumor-bearing mice survived significantly longer than control animals that retain c-RAF expression. Indeed, postmortem analysis of these mice revealed that they did not die of tumor burden, suggesting the existence of subtle long-term toxicities caused by the combined effect of widespread loss of c-RAF expression, the known deleterious effects of prolonged TMX exposure, and the old age of the treated animals. Yet, we did not observe significant weight loss or obvious toxic effects upon detailed examination of various tissues. Whereas these observations need to be taken into consideration when targeting c-RAF in the clinic, they are of limited concern since therapeutic strategies in a clinical setting are unlikely to result in irreversible loss of c-RAF expression.

More importantly, our results are in sharp contrast with the immediate death caused by the systemic elimination of the MEK1/2 or ERK1/2 kinases (Blasco et al., 2011). Interestingly, pharmacological inhibition of K-RAS-driven tumors in GEM models by MEK inhibitors is reasonably well tolerated and results in significant therapeutic response, highlighting the substantial differences between genetic and pharmacological inhibition of therapeutic targets (Samatar and Poulikakos, 2014). Unfortunately, MEK inhibitors have failed in the clinic, at least for the treatment of K-RAS mutant tumors, indicating that humans are more sensitive to these compounds than rodents. Thus, effective inhibition of K-RAS oncogenic signaling by blocking the MEK/ERK kinases in the clinic will depend on the existence of a narrow window between their anti-tumor effect and tolerable toxicities, a scenario not too different from that observed with classical cytotoxic compounds. In contrast, our data suggest that selective tampering with c-RAF will be better tolerated in the clinic. Moreover, we have not observed any tumor relapse after long-term exposure to TMX, suggesting the absence of relevant resistance mechanisms that could bypass the therapeutic benefit provided by the absence of c-RAF expression. Yet, c-RAF ablation by itself is not sufficient to induce complete regression of most tumors, hence suggesting that pharmacological targeting of c-RAF may not be sufficient to provide optimal therapeutic benefit to lung cancer patients and may have to be combined with other targeted therapies.

The differential toxic effects caused by ablation of c-RAF versus MEK1/2 or ERK1/2 may be due to the differential mechanisms by which they induce tumor regression. Indeed, our results suggest that the therapeutic effect observed upon c-RAF ablation is mediated by pathway(s) other than the MEK/ERK signaling cascade. Thus, the observed therapeutic activity is likely to result from the inability of c-RAF protein to interact with other partners. There is abundant evidence that c-RAF inhibits apoptosis in a kinase-independent manner. At least three partners have been implicated in this activity, including the mitochondrial BCL2 protein and the pro-apoptotic kinases ASK1 and MST2 (Matallanas et al., 2011). In agreement with these observations, ablation of c-RAF expression in both tumor tissue and cultured tumor cells readily induces activation of Caspase 3, a direct effector of apoptosis. Other c-RAF kinase-independent targets, such as ROKα, have been implicated in cell differentiation. Inactivation of ROKα has been shown to play a role on the pro-tumoral effect of c-RAF in SOS-induced skin tumors (Ehrenreiter et al., 2009). Our observation that c-RAF ablation activates ROKα as determined by the increased levels of phospho-Cofilin, also suggests that this kinase might be a key effector in c-RAF-mediated *Kras*^{G12V}/*Trp53*-driven tumor progression.

We were surprised by the differential therapeutic responses that c-*Raf* targeting induced across the battery of *Kras*^{G12V}/*Trp53* mutant tumors, considering the minimal differences among the genetic background of the mice and the identical nature of the driver mutations. Some of this variability was due to the differential extent of Cre-induced recombination of the conditional c-*Raf*^{L} alleles. Indeed, incomplete recombination was responsible for some, albeit not all, progressing tumors as well as for the remaining tumor cells in some of the regressing tumors. Several tumors, however, underwent elimination of c-RAF expression in most of their cells. Yet, most of these tumors retained significant levels of phospho-MEK and/or phospho-ERK expression. Only one tumor was completely devoid of both phospho-MEK and phospho-ERK. Similar results were observed with the tumor cell lines where c-RAF ablation did not affect MAPK activity. These results, taken together, illustrate that ablation of c-RAF in K-RAS mutant tumors can be uncoupled form MAPK signaling.

In summary, these studies demonstrate that c-RAF is a key mediator of *Kras*^{G12V}/*Trp53*-driven lung tumor progression by kinase-independent mechanism(s) and hence represents a suitable therapeutic target that, so far, has received little attention from the pharmaceutical industry. Targeting c-RAF in the clinic could be accomplished by inhibiting its kinase activity; however, this strategy would require certain levels of selectivity since concomitant inhibition of the B-RAF kinase will increase undesired toxicity. Moreover, complete elimination of the three RAF kinases in mice causes their rapid death (our unpublished data), a result that suggests that additional tampering with the A-RAF kinase will further increase undesirable toxic effects. Thus, the use of degron chemistry (Raina and Crews, 2010) will provide better opportunities for selectivity. As illustrated here, c-RAF inhibition is unlikely to result in complete tumor regression in the clinical setting, suggesting the need of combined therapies. Yet, targeting c-RAF will offer significant advantages over targeting other members of the MAPK pathway, such as the MEK and ERK kinases, due to the significantly milder toxic consequences and, possibly, the absence of resistance mechanisms.

STAR★METHODS

Detailed methods are provided in the online version of this paper and include the following:

- KEY RESOURCES TABLE
- CONTACT FOR REAGENT AND RESOURCE SHARING
- EXPERIMENTAL MODEL AND SUBJECT DETAILS
  - Mice
  - Patient Derived Xenograft (PDX) Models
  - Generation of *Kras*$^{+/FSFG12V}$ Mice
  - Cell Proliferation and Time Course Assays in Murine Cell Lines

- Cell Proliferation Assay and Orthotopic Implantation of Human Lung Tumor Cell Lines
- Colony Formation Assay
- METHOD DETAILS
  - Tumor Induction and Tamoxifen Exposure
  - Micro CT and PET-CT Imaging
  - Histopathology and Immunohistochemistry
  - Southern Blot Analysis
  - Western Blot Analysis
- QUANTIFICATION AND STATISTICAL ANALYSIS

SUPPLEMENTAL INFORMATION

Supplemental Information includes six figures and can be found with this article online at https://doi.org/10.1016/j.ccell.2017.12.014.

ACKNOWLEDGMENTS

We thank David Kirsch for providing the *Trp53*$^{F/F}$ strain. We thank Dr. Manuel Morente for his advice in histopathological analysis. We also thank M. San Roman, C. Lechuga, R. Villar, P. Villanueva, N. Cabrera, J. Condo, M. Munoz, and R. Blasco for excellent technical support. This work was supported by grants from the European Research Council (ERC-2009-AdG/250297-RAS AHEAD and ERC-2015-AdG/695566, THERACAN), EU-Framework Program (HEALTH-F2-2010-259770/LUNGTARGET and HEALTH-2010-260791/EUROCANPLATFORM), Spanish Ministry of Economy and Competitiveness (SAF2011-30173 and SAF2014-59864-R) and Autonomous Community of Madrid (S2011/BDM-2470/ONCOCYCLE) to M.B. M.B. is a recipient of an Endowed Chair from the AXA Research Fund. M.S. is the recipient of an FPU fellowship from the Spanish Ministry of Education. S.F. was supported by a FEBS Long-Term Fellowship and a Sara Borrell grant from the Instituto de Salud Carlos III. L.E.-B. is the recipient of an FPI fellowship from the Spanish Ministry of Economy and Competitiveness.

AUTHOR CONTRIBUTIONS

M.M. and M.B. designed experiments and research aims, analyzed data, and wrote the manuscript with help from co-authors. M.S., S.F., L.E.-B., E.B.-M., and M.M. performed experiments and analyzed the data. M. Djurec performed experiments with hematopoietic cells. P.P.L.-C. and M.H. provided human samples. M. Drosten generated the *Kras*^{FSFG12V} allele. M. Drosten, C.G., P.P.L.-C. contributed critical information and helpful discussions.

DECLARATION OF INTERESTS

The authors declare no competing interests.

Received: July 6, 2017
Revised: October 24, 2017
Accepted: December 21, 2017
Published: January 25, 2018

REFERENCES

Blasco, R.B., Francoz, S., Santamaria, D., Canamero, M., Dubus, P., Charron, J., Baccarini, M., and Barbacid, M. (2011). c-Raf, but not B-Raf, is essential for development of K-Ras oncogene-driven non-small cell lung carcinoma. Cancer Cell *19*, 652–663.

Buchholz, F., Angrand, P.O., and Stewart, A.F. (1998). Improved properties of FLP recombinase evolved by cycling mutagenesis. Nat. Biotechnol. *16*, 657–662.

Castellano, E., and Downward, J. (2011). RAS interaction with PI3K: more than just another effector pathway. Genes Cancer *2*, 261–274.

Castellano, E., Sheridan, C., Thin, M.Z., Nye, E., Spencer-Dene, B., Diefenbacher, M.E., Moore, C., Kumar, M.S., Murillo, M.M., Grönroos, E., et al. (2013). Requirement for interaction of PI3-kinase p110alpha with RAS in lung tumor maintenance. Cancer Cell *24*, 617–630.

Cox, A.D., Fesik, S.W., Kimmelman, A.C., Luo, J., and Der, C.J. (2014). Drugging the undruggable RAS: mission possible? Nat. Rev. Drug Discov. *13*, 828–851.

Chen, A.P., Ohno, M., Giese, K.P., Kuhn, R., Chen, R.L., and Silva, A.J. (2006). Forebrain-specific knockout of B-raf kinase leads to deficits in hippocampal long-term potentiation, learning, and memory. J. Neurosci. Res. *83*, 28–38.

Chen, Z., Fillmore, C.M., Hammerman, P.S., Kim, C.F., and Wong, K.K. (2014). Non-small-cell lung cancers: a heterogeneous set of diseases. Nat. Rev. Cancer *14*, 535–546.

Dewan, N.A., Gupta, N.C., Redepenning, L.S., Phalen, J.J., and Frick, M.P. (1993). Diagnostic efficacy of PET-FDG imaging in solitary pulmonary nodules. Potential role in evaluation and management. Chest *104*, 997–1002.

DuPage, M., and Jacks, T. (2013). Genetically engineered mouse models of cancer reveal new insights about the antitumor immune response. Curr. Opin. Immunol. *25*, 192–199.

DuPage, M., Mazumdar, C., Schmidt, L.M., Cheung, A.F., and Jacks, T. (2012). Expression of tumour-specific antigens underlies cancer immunoediting. Nature *482*, 405–409.

Ehrenreiter, K., Kern, F., Velamoor, V., Meissl, K., Galabova-Kovacs, G., Sibilia, M., and Baccarini, M. (2009). Raf-1 addiction in Ras-induced skin carcinogenesis. Cancer Cell *16*, 149–160.

Guerra, C., Mijimolle, N., Dhawahir, A., Dubus, P., Barradas, M., Serrano, M., Campuzano, V., and Barbacid, M. (2003). Tumor induction by an endogenous K-ras oncogene is highly dependent on cellular context. Cancer Cell *4*, 111–120.

Huser, M., Luckett, J., Chiloeches, A., Mercer, K., Iwobi, M., Giblett, S., Sun, X.M., Brown, J., Marais, R., and Pritchard, C. (2001). MEK kinase activity is not necessary for Raf-1 function. EMBO J. *20*, 1940–1951.

Jackson, E.L., Olive, K.P., Tuveson, D.A., Bronson, R., Crowley, D., Brown, M., and Jacks, T. (2005). The differential effects of mutant p53 alleles on advanced murine lung cancer. Cancer Res. *65*, 10280–10288.

Jesenberger, V., Procyk, K.J., Ruth, J., Schreiber, M., Theussl, H.C., Wagner, E.F., and Baccarini, M. (2001). Protective role of Raf-1 in *Salmonella*-induced macrophage apoptosis. J. Exp. Med. *193*, 353–364.

Kamata, T., Giblett, S., and Pritchard, C. (2017). KRASG12D expression in lung-resident myeloid cells promotes pulmonary LCH-like neoplasm sensitive to statin treatment. Blood *130*, 514–526.

Karreth, F.A., Frese, K.K., DeNicola, G.M., Baccarini, M., and Tuveson, D.A. (2011). C-Raf is required for the initiation of lung cancer by K-Ras(G12D). Cancer Discov. *1*, 128–136.

Lee, C.L., Moding, E.J., Huang, X., Li, Y., Woodlief, L.Z., Rodrigues, R.C., Ma, Y., and Kirsch, D.G. (2012). Generation of primary tumors with Flp recombinase in FRT-flanked p53 mice. Dis. Model. Mech. *5*, 397–402.

Matallanas, D., Birtwistle, M., Romano, D., Zebisch, A., Rauch, J., von Kriegsheim, A., and Kolch, W. (2011). Raf family kinases: old dogs have learned new tricks. Genes Cancer *2*, 232–260.

Mikula, M., Schreiber, M., Husak, Z., Kucerova, L., Ruth, J., Wieser, R., Zatloukal, K., Beug, H., Wagner, E.F., and Baccarini, M. (2001). Embryonic lethality and fetal liver apoptosis in mice lacking the c-raf-1 gene. EMBO J. *20*, 1952–1962.

Niault, T.S., and Baccarini, M. (2010). Targets of raf in tumorigenesis. Carcinogenesis *31*, 1165–1174.

Ostrem, J.M., Peters, U., Sos, M.L., Wells, J.A., and Shokat, K.M. (2013). K-Ras(G12C) inhibitors allosterically control GTP affinity and effector interactions. Nature *503*, 548–551.

Puyol, M., Martin, A., Dubus, P., Mulero, F., Pizcueta, P., Khan, G., Guerra, C., Santamaria, D., and Barbacid, M. (2010). A synthetic lethal interaction between K-Ras oncogenes and Cdk4 unveils a therapeutic strategy for non-small cell lung carcinoma. Cancer Cell *18*, 63–73.

Raina, K., and Crews, C.M. (2010). Chemical inducers of targeted protein degradation. J. Biol. Chem. *285*, 11057–11060.

Ruzankina, Y., Pinzon-Guzman, C., Asare, A., Ong, T., Pontano, L., Cotsarelis, G., Zediak, V.P., Velez, M., Bhandoola, A., and Brown, E.J. (2007). Deletion of the developmentally essential gene ATR in adult mice leads to age-related phenotypes and stem cell loss. Cell Stem Cell *1*, 113–126.

Samatar, A.A., and Poulikakos, P.I. (2014). Targeting RAS-ERK signalling in cancer: promises and challenges. Nat. Rev. Drug Discov. *13*, 928–942.

Scheffler, M., Zander, T., Nogova, L., Kobe, C., Kahraman, D., Dietlein, M., Papachristou, I., Heukamp, L., Büttner, R., Boellaard, R., et al. (2013). Prognostic impact of [18F]fluorothymidine and [18F]fluoro-D-glucose baseline uptakes in patients with lung cancer treated first-line with erlotinib. PLoS One *8*, e53081.

Sebolt-Leopold, J.S., and Herrera, R. (2004). Targeting the mitogen-activated protein kinase cascade to treat cancer. Nat. Rev. Cancer *4*, 937–947.

Wojnowski, L., Zimmer, A.M., Beck, T.W., Hahn, H., Bernal, R., Rapp, U.R., and Zimmer, A. (1997). Endothelial apoptosis in Braf-deficient mice. Nat. Genet. *16*, 293–297.

STAR★METHODS

KEY RESOURCES TABLE

REAGENT or RESOURCE	SOURCE	IDENTIFIER
Antibodies		
Mouse monoclonal anti-B-Raf	Santa Cruz Biotechnolgy	Cat# sc-5284; RRID: AB_626760
Mouse monoclonal anti-c-Raf	BD Biosciences	Cat# 610151; RRID: AB_397552
Rabbit polyclonal anti-Mek1	Santa Cruz Biotechnology	Cat# sc-219; RRID: AB_631921
Rabbit monoclonal anti-Phospho-Mek1/Mek2	Cell Signaling	Cat# 9154; RRID: AB_2138017
Mouse monoclonal anti-Erk-1	BD Pharmingen	Cat# 554100; RRID: AB_395238
Mouse monoclonal anti-Erk-2	BD Biosciences	Cat# 610103; RRID: AB_397509
Rabbit polyclonal anti-Phospho-Erk1/Erk2	Cell Signaling	Cat# 9101; RRID: AB_331646
Rabbit polyclonal anti-Akt	Cell Signaling	Cat# 9272; RRID: AB_329827
Rabbit monoclonal anti-Phospho-Akt	Cell Signaling	Cat# 4060; RRID: AB_2315049
Mouse monoclonal anti-Pan-Ras	Calbiochem	Cat# OP40; RRID: AB_213400
Rabbit polyclonal anti-Caspase 3	Cell Signaling	Cat# 9662; RRID: AB_331439
Rabbit polyclonal anti-Cleaved-Caspase 3	Cell Signaling	Cat# 9661; RRID: AB_2341188
Goat polyclonal anti-Phospho-Cofilin	Santa Cruz	Cat# sc-21867-R; RRID: AB_2080618
Mouse monoclonal anti-CD3ε	Santa Cruz	Cat# sc1127; RRID: AB_631128
Rabbit polyclonal anti-CD8	Santa Cruz	Cat# sc7188; RRID: AB_638273
Mouse monoclonal anti-Gapdh	Sigma	Cat# G8795; RRID: AB_1078991
Mouse monoclonal anti-Vinculin	Sigma	Cat# V9131; RRID: AB_477629
Rabbit monoclonal anti-Ki67	Master Diagnostica	Cat# 0003110QD; RRID: AB_2314696
Rat monoclonal anti-F4/80	ABD Serotec	Cat# MCA497; RRID: AB_2098196
Bacterial and Virus Strains		
Ad-Flp	Homemade	N/A
Chemicals, Peptides, and Recombinant Proteins		
4-hydroxy-Tamoxifen	Sigma	Cat# H7904
Tam400/CreER diet	ENVIGO	Cat# TD55125
Puromycin	Invivogen	Cat# ant-pr-1
Blasticidin	EDM Millipore Corp	Cat# 203350
Matrigel Matrix	Corning	Cat# 354234
Ketamine	Merial Laboratorios	N/A
Xylazine	Bayer	N/A

(*Continued on next page*)

Continued		
REAGENT or RESOURCE	SOURCE	IDENTIFIER
[^{18}F]-fluoro-2-deoxy-glucose ([^{18}F]-FDG)	ITP Cyclotron (Madrid)	N/A
Phosphatase Inhibitor Cocktail 2	Sigma	Cat# P5726
Phosphatase Inhibitor Cocktail 3	Sigma	Cat# P0044
cOmplete Mini	Roche	Cat# 11836153001
Bradford	Bio-Rad	Cat# 500-0006
PstI enzyme	New England Biolabs	Cat# R0140S
Experimental Models: Cell Lines		
Murine K-*Ras*^{G12V};*Trp53*$^{-/-}$;h*UBC-CreERT2*$^{+/T}$;c-*Raf*$^{L/L}$	This paper	N/A
PDX-derived cell line 1 (PDX-dc1)	This paper	N/A
PDX-derived cell line 2 (PDX-dc2)	This paper	N/A
Experimental Models: Organisms/Strains		
Mouse: B6.129-Krastm3Bbd/J (K-Ras$^{+/FSFG12V}$)	This paper (The Jackson Laboratory)	Cat# 027010
Mouse: B6;129-Trp53tm1.1Dgk/J (*Trp53*$^{F/F}$)	The Jackson Laboratory	Cat# 017767
Mouse: *RERT* $^{ert/ert}$	(Guerra et al., 2003)	N/A
Mouse: B6.Cg-Tg(UBC-cre/ERT2)1Ejb/1J (h*UBC-CreERT2*$^{+/T}$)	The Jackson Laboratory	Cat# 007001
Mouse: 129-Braftm1Sva/J (B-*Raf*$^{L/L}$)	The Jackson Laboratory	Cat# 006373
Mouse: c-Raf $^{L/L}$	(Jesenberger et al., 2001)	N/A
Hsd: Athymic Nude-Foxn1nu	Harlan	N/A
Oligonucleotides		
Forward wild-type Primer: 5'-CCACAGGGTATAGCGTACTATGCAG-3'	This paper	N/A
Forward mutant Primer: 5'-TAGTGCCTTGACTAGAGATCA-3'	This paper	N/A
Reverse Primer: 5'-CTCAGTCATTTTCAGCAGGC-3'	This paper	N/A
Recombinant DNA		
pLKO.1-puro Scrambled shRNA	Sigma Aldrich	Cat# shc002
pLKO.1-blast Scrambled shRNA	This paper	N/A
pLKO.1-puro c-RAF shRNA	Sigma Aldrich	Cat# TRCN0000001065
pLKO.1-blast c-RAF shRNA	This paper	N/A
pLVX-puro	Clonetech	Cat# 632164
pLVX-puro c-Raf WT	This paper	N/A
Software and Algorithms		
MMWS software (eXplore Vista)	N/A	N/A
3D OSEM reconstruction algorithm	N/A	N/A
Graphpad Prism 5.01	N/A	N/A
Panomaric Viewer 1.15.3 software (3dhistech)	N/A	N/A
AxioVision 4.6 software (Zeiss)	N/A	N/A
Other		
NUPAGE ^{TM} 4-12% Bis-Tris Midi Gel	Invitrogen	Cat# WG1402
Nitrocellulose Blotting Membrane	GE Healthcare	Cat# 10600001

CONTACT FOR REAGENT AND RESOURCE SHARING

Further information and request for resources and reagents should be directed to and will be fulfilled by the Lead Contact, Monica Musteanu (mmusteanu@cnio.es).

EXPERIMENTAL MODEL AND SUBJECT DETAILS

Mice

The generation of *Kras*$^{+/FSFG12V}$ strain is described below. Compound mice using the following transgenes were generated for this study: *Trp53*$^{F/F}$ (Lee et al., 2012), *RERT*$^{ert/ert}$ (Guerra et al., 2003), h*UBC-CreERT2*$^{+/T}$ (Ruzankina et al., 2007), *Braf*$^{L/L}$ (Chen et al., 2006) and c-*Raf*$^{L/L}$ (Jesenberger et al., 2001). All animal experiments were approved by the Ethical Committees of the Spanish National Cancer Research Centre (CNIO), the Carlos III Health Institute, and the Autonomous Community of Madrid (PROEX 270/14) and were performed in accordance with the guidelines stated in the International Guiding Principles for Biomedical Research Involving Animals, developed by the Council for International Organizations of Medical Sciences (CIOMS). Mice were housed in specific-pathogen-free conditions at CNIO's Animal Facility (AAALAC, JRS:dpR 001659). Female and male mice were used for the experiments.

Patient Derived Xenograft (PDX) Models

Primary tumors were obtained from Hospital HM Sanchinaro with approval by the Ethical Committee (CEIC HM Hospitales, (FHM.06.10) and ethical and legal protection guidelines of human subjects, including informed consent, were followed. PDX1: male, 60 years old and PDX2: female, 54 years old.

Generation of *Kras*$^{+/FSFG12V}$ Mice

The targeting vector was generated by Taconic Artemis (Cologne, Germany). Briefly, the homology arms including the first exon that contains the oncogenic G12V mutation (GGT [Gly] to GTA [Val]) were amplified by PCR using as a template a targeting vector previously developed to generate the *Kras*^{LSLG12Vgeo} allele (Guerra et al., 2003). A PGK-Neo-STOP cassette was generated by PCR amplification of the 1377 bp STOP cassette derived from the *Kras*^{LSLG12Vgeo} targeting vector with primers that incorporated NdeI restriction sites at the termini of the PCR product. The STOP cassette was subsequently cloned into the NdeI restriction site of pBASIC10 (Taconic Artemis) which contained a PGK-Neo cassette followed by an NdeI restriction site flanked by frt sequences. The left homology arm was cloned as a 3019 bp NotI/BstEII fragment where an internal BstEII site was previously disabled by site-directed mutagenesis. The 1867 bp right homology arm including the mutated exon 1 was PCR-amplified from the *Kras*^{LSLG12Vgeo} targeting vector with primers that incorporated AscI and PmeI restriction sites to the termini of the PCR product. This fragment was finally cloned into the corresponding AscI/PmeI restriction sites to assemble the *Kras*^{FSFG12V} targeting vector. All sequences amplified by PCR were verified by DNA sequencing. The resulting targeting vector was linearized with NotI and electroporated into Art4.12 (B6129S6F1) ES cells. 288 G418-resistant clones were submitted to Southern blot analysis to identify those clones that had undergone the expected recombination event (4 positive clones; recombination frequency 1%). Two independent recombinant ES cell clones were microinjected into C57BL/6J blastocysts and transplanted into pseudo-pregnant females. Chimeric mice were backcrossed to C57BL/6J mice and germ line transmission of the targeted allele was confirmed by Southern blot analysis. The resulting *Kras*$^{+/FSFG12V}$ mice were maintained in a mixed 129Sv/J x C57BL/6J background. For PCR genotyping the following primers were used: (i) forward wild-type primer (5'- CCACAGGGTATAGCGTACTATGCAG-3'), (ii) forward mutant primer (5'-TAGTGCCTTGACTAGAGATCA-3') and (iii) reverse primer (5'-CTCAGTCATTTTCAGCAGGC-3') yielding a 358 bp DNA fragment for the wild-type allele and 507 bp DNA fragment for the targeted *Kras*^{FSFG12V} allele. *Kras*$^{+/FSFG12V}$ mice are available at The Jackson Laboratory (B6.129-*Kras*^{tm3Bbd}/J).

Cell Proliferation and Time Course Assays in Murine Cell Lines

To evaluate the effect of c-RAF ablation on apoptosis *Kras*^{G12V};*Trp53*$^{-/-}$;h*UBC-CreERT2*$^{+/T}$;c-*Raf*$^{L/L}$ tumor cells were maintained at 37°C in DMEM (GIBCO) medium containing 10% FBS (GIBCO) and 600 nM (4-hydroxy-tamoxifen) 4OHT (Sigma, H7904) for 4 days. Cells were harvested at 0, 8, 24, 48, 72 and 96 hours post exposure to 4OHT and cell lysates were analyzed by Western Blot. All 3 tumoral cell lines used were obtained from 7 month old male animals.

Cell Proliferation Assay and Orthotopic Implantation of Human Lung Tumor Cell Lines

To assess the influence of c-RAF in cell proliferation we isolated 2 PDX-derived cell lines (PDX-dc) from the upper described PDX models. Cell lines were maintained at 37°C in DMEM (GIBCO) supplemented with 10% FBS (GIBCO). These cells were infected with pLKO.1-puro lentiviral supernatants expressing a shRNA against c-RAF and a scrambled shRNA and selected with puromycin (2 μg/ml, Invitrogen) for 48 hr. Once selection was finished, 30,000 cells were seeded in 6-well plates and counted in triplicates by using Neubauer chambers. Scrambled shRNA sequence: CCGGGCGCGATAGCGCTAATAATTTCTCGAGAAATTATTAGCGCTATCGCGC

TTTTT and shRNA against c-RAF sequence: CCGGGCTTCCTTATTCTCACATCAA

CTCGAGTTGATGTGAGAATAAGGAAGCTTTTT. For the in vivo orthotopic tumor model 100,000 cells in 10 μl (1:1) PBS:Matrigel Matrix (Corning, 354234) infected as above were injected directly into the lungs of 6 week old nude (*Foxn1*$^{nu/nu}$) female mice (Harlan). Each PDX-dc-injected group of mice was sacrificed at the same time. PDX-dc1 injected mice were sacrificed at 5 weeks and PDX-dc2-injected ones at 3 weeks. Tumors were counted and caliper-measured post-mortem in each case.

Colony Formation Assay

To evaluate potential effect of c-RAF in rescuing cell proliferation, PDX-dc1-derived cells were infected with pLVX-puro lentiviral supernatants expressing wild-type murine c-*Raf* or an empty vector and selected by addition of puromycin (2 μg/ml, Invitrogen) for 48h.

Then, these cells were infected with pLKO.1-blast lentiviral supernatants expressing a shRNA against c-RAF and a scrambled shRNA as control and selected by addition of blasticidin (4 μg/ml, EDM Millipore Corp) for 72 hr. Once selection was finished, 10,000 cells were seeded in 10 cm diameter dishes and stained after 2 weeks by using 0.2% Crystal Violet. Colonies were counted and quantified.

METHOD DETAILS

Tumor Induction and Tamoxifen Exposure

Induction of lung adenocarcinomas was carried out in anesthetized (i.p. injection of: ketamine 75 mg/kg, xylazine 12 mg/kg) 8 to 10-week old mice by intratracheal instillation of a single dose of 10^6 pfu of adeno viruses encoding the Flp recombinase (Ad-Flp). Activation of the inducible CreERT2 recombinase encoded by the h*UBC-CreERT2* transgene was carried out by feeding the mice with a TMX-containing diet (Teklad CRD TAM400 diet, Harlan) *ad libitum* during the duration of the experiment.

Micro CT and PET-CT Imaging

Lung images were acquired using the eXplore Vista PET-CT (GE Healthcare). MicroCT images consisted of 400 projections collected in one full rotation of the gantry in approximately 10 min. CT images were reconstructed using filtered back projection with a Shepp–Logan filter. For PET imaging, mice were injected with 15 MBq of ^{18}F-FDG into the lateral tail vein. PET images were reconstructed using 3D OSEM reconstruction algorithm. For PET quantification, regions of interest were drawn over the tumors using the MMWS/Vista software (GE Healthcare). The standardized uptake value (SUV) was calculated using the following formula: SUV = Tissue radioactivity concentration (MBq/cm^3) / (injected dose (MBq) / body weight (g)).

Histopathology and Immunohistochemistry

For routine histological study, lung lobes were fixed in 10%-buffered formalin (Sigma) and embedded in paraffin. Tumors were counted and classified according to standard histopathological grading discriminating between benign (adenoma) and malignant (adenocarcinoma) tumors. Tumor grading (stage II to V) was determined as previously described (Jackson et al., 2005). Antibodies used for immunostaining included those raised against: Ki67 (Master Diagnostica, 0003110QD), phospho-ERK (Cell Signaling, 9101), cleaved Caspase3 (Cell Signaling, 9661), and phospho-Cofilin (Santa Cruz, sc-21867-R), CD3ε (Santa Cruz, sc-1127), F4/80 (ABD Serotec, MCA497). Haematoxilin and eosin (H&E) and immune-stained tissue slides were scanned using the Mirax scanner (Zeiss) and photos were exported using the Panoramic Viewer 1.15.3 software (3dhistech). Immunostainings were quantified using the AxioVision 4.6 software (Zeiss).

Southern Blot Analysis

For the detection of c-*Raf*^{L} and c-*Raf*$^{-}$ alleles genomic DNA was digested with PstI and probed with an 854 bp DNA fragment corresponding to sequences located in intron 4 downstream from the second loxP site resulting in diagnostic bands of 3.1 kbp for the c-*Raf*^{L} and 3.5 kbp for the c-*Raf*$^{-}$ alleles respectively.

Western Blot Analysis

Protein extraction was performed in protein lysis buffer (50 mM Tris-HCl pH 7.4, 150 mM NaCl, 0.5% NP-40) supplemented with a cocktail of protease and phosphatase inhibitors (cOmplete Mini, Roche; Phosphatase Inhibitor Cocktail 2 and 3, Sigma). To quantify the amount of protein obtained the Bradford (Bio-Rad) method was used. 25 μg of protein extracts obtained from tumor tissue were separated on NUPAGE™ 4-12% Bis-Tris Midi gels (Invitrogen), transferred to a nitrocellulose membrane (GE Healthcare) and blotted with antibodies raised against B-RAF (Santa Cruz, sc-5284), c-RAF (BD Biosciences, 610151), MEK1 (Santa Cruz, sc-219), phospho-MEK (Cell Signaling, 9154), ERK1 (BD Pharmingen, 554100), ERK2 (BD Biosciences, 610103), phospho-ERK (Cell Signaling, 9101), AKT (Cell Signaling, 9272), phospho-AKT (Cell Signaling, 4060), pan-RAS (Calbiochem, OP40), Caspase 3 (Cell Signaling, 9662), cleaved Caspase 3 (Cell Signaling, 9661), CD3ε (Santa Cruz, sc-1127), CD8α (Santa Cruz, sc-7188), GAPDH (Sigma, G8795) and Vinculin (Sigma, V9131). Primary antibodies were detected with goat secondary antibodies directed against mouse or rabbit IgGs (HRP, Dako and Alexa Fluor 680, Invitrogen) and visualized with ECL Western Blot detection solution (GE Healthcare) or Odyssey infrared imaging system (*LI-COR* Biosciences).

QUANTIFICATION AND STATISTICAL ANALYSIS

All values are expressed as mean ±SEM. p values were calculated with the unpaired Student's t test using the GraphPad Prism (Version 5.01) software. A p value ≤ 0.05 is considered statistically significant. Significant differences between experimental groups were: *$p < 0.05$, **$p < 0.01$ or ***$p < 0.001$.